

Modelled trends in Antarctic sea ice thickness

**Paul R. Holland¹, Nicolas Bruneau^{1*}, Clare Enright², Martin Losch³, Nathan T. Kurtz⁴,
and Ron Kwok⁵**

¹British Antarctic Survey, Cambridge, UK.

²Tyndall Centre for Climate Change Research, University of East Anglia, Norwich, UK.

³Alfred Wegener Institute for Polar and Marine Research, Bremerhaven, Germany.

⁴NASA Goddard Space Science Center, Maryland, USA.

⁵Jet Propulsion Laboratory, Pasadena, California, USA.

Corresponding author address: Paul Holland, British Antarctic Survey, High Cross,
Madingley Road, Cambridge, CB3 0ET, UK. E-mail: p.holland@bas.ac.uk

* Now at: RMS Ltd., London, UK.

Abstract

1 Unlike the rapid sea-ice losses reported in the Arctic, satellite observations show an overall
2 increase in Antarctic sea ice concentration over recent decades. However, observations of
3 decadal trends in Antarctic ice thickness, and hence ice volume, do not currently exist. In
4 this study a model of the Southern Ocean and its sea ice, forced by atmospheric reanalyses, is
5 used to assess 1992—2010 trends in ice thickness and volume. The model successfully
6 reproduces observations of mean ice concentration, thickness, and drift, and decadal trends in
7 ice concentration and drift, imparting some confidence in the hindcasted trends in ice
8 thickness. The model suggests that overall Antarctic sea ice volume has increased by
9 approximately $30\text{km}^3/\text{y}$ ($0.4\%/\text{y}$) as an equal result of areal expansion ($20\times 10^3\text{km}^2/\text{y}$, or
10 $0.2\%/\text{y}$) and thickening ($1.5\text{mm}/\text{y}$, or $0.2\%/\text{y}$). This ice volume increase is an order of
11 magnitude smaller than the Arctic decrease, and about half the size of the increased
12 freshwater supply from the Antarctic Ice Sheet. Similarly to the observed ice concentration
13 trends, the small overall increase in modelled ice volume is actually the residual of much
14 larger opposing regional trends. Thickness changes near the ice edge follow observed
15 concentration changes, with increasing concentration corresponding to increased thickness.
16 Ice thickness increases are also found in the inner pack in the Amundsen and Weddell seas,
17 where the model suggests that observed ice-drift trends directed towards the coast have
18 caused dynamical thickening in autumn and winter. Modelled changes are predominantly
19 dynamic in origin in the Pacific sector and thermodynamic elsewhere.

20

21 **1. Introduction**

22 Arctic sea ice extent has declined rapidly in recent decades ($-52 \times 10^3 \text{ km}^2/\text{y}$ for 1979-2010),
23 but Antarctic sea ice extent has slowly increased ($+17 \times 10^3 \text{ km}^2/\text{y}$) over the same period
24 (Cavalieri and Parkinson 2012; Comiso and Nishio 2008; Parkinson and Cavalieri 2012;
25 Zwally et al. 2002), raising fundamental questions of why the two poles have evolved so
26 differently in the context of climate change. The small overall Antarctic increase in ice area
27 is actually the residual of a coherent pattern of much larger regional increases and decreases
28 that almost compensate each other. These large local areal changes (up to 2% per year
29 increase and decrease, or 60% total over 30 years; Turner et al. (2009)) can also be viewed as
30 changes in the length of the ice season (up to 3 days per year, or 3 months in total;
31 Stammerjohn et al. (2012)). The local changes are of the same magnitude as those in the
32 Arctic, which does not feature the regions of ice expansion that, in the Antarctic, more than
33 offset the regions of loss.

34

35 It is currently unclear exactly what causes the regional pattern of changes that produces the
36 overall increase in ice cover. Proposed drivers include changes in atmospheric temperature
37 or wind stress (Lefebvre and Goosse 2005; Liu et al. 2004; Turner et al. 2009), precipitation
38 (Liu and Curry 2010), ocean temperature (Jacobs and Comiso 1997), atmosphere and ocean
39 feedbacks (Stammerjohn et al. 2008; Zhang 2007), and increased freshwater flux from the
40 Antarctic Ice Sheet (Bintanja et al. 2013). Recent work has shown that the trends in Antarctic
41 ice concentration are associated with trends in ice drift, and that both are caused by changes
42 in near-surface winds through a combination of dynamic and thermodynamic effects
43 (Holland and Kwok 2012). However, the ultimate cause of the relevant wind changes
44 remains uncertain.

45

46 The current generation of coupled climate models are unable to capture the increase in overall
47 Antarctic sea ice extent, instead hindcasting a decline in ice cover of a similar magnitude to
48 their modelled Arctic (Turner et al. 2012). This suggests that important deficiencies exist in
49 our understanding of ice and climate physics that will be relevant to the prediction of climate
50 at both poles. The model projections of most aspects of Antarctic climate are questionable if
51 they cannot reproduce past observations of sea ice extent, since it is one of the better-
52 monitored polar climate variables. Improved climate models are also required to answer top-
53 level questions about past changes in Antarctic sea ice that are of vital importance to
54 policymakers. For example, it is unclear why Antarctic sea ice is not rapidly declining in
55 response to increased greenhouse-gas concentrations and depletion of stratospheric ozone,
56 both of which are found to decrease Antarctic sea ice in coupled climate models (Bitz et al.
57 2006; Sigmond and Fyfe 2010). Several studies have suggested that the observed increase is
58 an unlikely result of natural variability, which would consequently only be captured by a
59 small proportion of simulations (Mahlstein et al. 2013; Polvani and Smith 2013; Swart and
60 Fyfe 2013). However, this result is marginal, valid only for the annual-mean circumpolar
61 trend (Swart and Fyfe 2013), and relies upon the models having realistic natural variability,
62 which is not the case (Turner et al. 2012; Zunz et al. 2013). In this study we investigate the
63 Antarctic ice trends further in a quest to provide additional insight into these model
64 weaknesses.

65

66 A critical gap in our understanding of Antarctic sea ice and its trends is caused by the relative
67 paucity of Antarctic ice thickness data. Though spatially widespread, in-situ observations are
68 severely lacking in spatial and temporal detail (Worby et al. 2008). Ice thickness can be
69 determined from satellite altimetry by measuring the ice freeboard and assuming that the ice
70 is freely floating with some choice of ice, snow, and seawater properties. Radar altimeters

71 have provided a relatively long record of ice thickness in the Arctic, but are subject to
72 variable snow penetration in the Antarctic that currently precludes the reliable determination
73 of ice freeboard (Giles et al. 2008). The freeboard of Antarctic ice and snow can be
74 accurately measured using laser altimeters, and this can be converted to ice thickness using
75 independent estimates of snow thickness and snow and ice density (Markus et al. 2011; Xie et
76 al. 2013; Zwally et al. 2008). Recent studies demonstrate that ice thickness can be derived to
77 a reasonable level of accuracy using the simple assumption that the snow—ice interface is at
78 sea level (Kurtz and Markus 2012; Ozsoy-Cicek et al. 2013). However, the available laser
79 altimeter data are limited in temporal coverage, and therefore unable to provide reliable
80 trends in ice thickness. Instead, we use a coupled ice—ocean model to investigate the ice
81 thickness trends and their drivers.

82

83 Models have previously been used to study various sensitivities of Antarctic sea ice,
84 including the effects of surface precipitation (Powell et al. 2005), winds (Stossel et al. 2011),
85 and ice-shelf meltwater (Hellmer 2004). Models have also been used to assess linkages
86 between sea-ice variability and large-scale climate modes (Lefebvre and Goosse 2005, 2008).
87 Several such models have been validated against ice observations, including those of ice
88 thickness, with notable success (Fichefet et al. 2003a; Losch et al. 2010; Timmermann et al.
89 2002; Timmermann et al. 2004; Timmermann et al. 2005; Timmermann et al. 2009).
90 However, only a few model studies consider changes in Antarctic sea ice thickness or
91 volume.

92

93 Proposing an ocean feedback on increasing Antarctic sea ice, Zhang (2007) simulated a 1979-
94 2004 increase in ice volume of $200 \text{ km}^3/\text{y}$. The mean ice area of 10^7 km^2 thus implies a
95 Antarctic-mean thickening of $2 \text{ cm}/\text{y}$, or 0.5 m over the period, which seems unfeasibly large.

96 This simulation had many shortcomings: overestimation of annual-mean ice volume by a
97 factor of 2 (Kurtz and Markus 2012); overestimation of area trend by a factor of 3;
98 disagreement with observed spatial pattern of concentration trends; disagreement with
99 observed temporal variability in total ice extent. Fichefet et al. (2003a) found an area
100 increase of $11 \times 10^3 \text{ km}^2/\text{y}$ over 1958-1999 but no appreciable trend in ice thickness, though
101 considerable wind-driven decadal variability in ice thickness and area were identified.
102 Fichefet et al. (2003b) investigated 1955-2001 area and volume trends, finding an overall
103 decrease of $9 \times 10^3 \text{ km}^2/\text{y}$ and increase of $11 \text{ km}^3/\text{y}$ respectively. However, reanalysis-forced
104 models should be treated with extreme caution prior to the onset of satellite sounding data
105 assimilation in late 1978 (Bromwich and Fogt 2004), and the latter model produces no trend
106 in ice area during 1978-2001. Timmermann et al. (2005) report little modelled trend in ice
107 area or volume during 1977-1999, attributing this to their spin-up technique of repeating the
108 reanalysis forcing twice. Timmermann et al. (2009) model an ice area increase of 11×10^3
109 km^2/y for 1979-2006 but do not report the corresponding volume trend. Crucially, the latter
110 four studies do not show the spatial distribution of ice concentration trends, so it is impossible
111 to assess whether the physical processes driving their overall trends are realistic.

112

113 A recent modelling study by Zhang (in press) specifically investigates the effect of changes in
114 winds on Antarctic ice volume. The study finds an increase in ice volume of $69 \text{ km}^3/\text{y}$ over
115 1979-2010, but at $15 \times 10^3 \text{ km}^3$ the annual mean ice volume in this model is approximately
116 twice that inferred from observation (Kurtz and Markus 2012), which casts significant doubt
117 on the value of the volume trend. Since the ice extent is reasonable, this implies that the ice
118 thickness is approximately twice the true value. The study does not examine in detail the
119 changes during different seasons, in different regions, or the thermodynamic and dynamic
120 mechanisms underlying the changes.

121

122 Probably the most reliable estimate of recent ice volume trends are from the model of
123 Massonnet et al. (2013), which formally optimises the estimate by assimilating ice
124 concentration data using an ensemble Kalman filter. The results show an overall 1980—2008
125 increase in ice volume of 36 ± 34 km³/y, with a regional pattern of ice-thickness trends that are
126 closely related to the changes observed in ice concentration. The use of data assimilation has
127 strengths and weaknesses; the results should be quantitatively as reliable as possible, but the
128 adjustments made to the model state vector do not have a directly physical origin, and none
129 of the ice or ocean variables are conserved (Massonnet et al. 2013; Mathiot et al. 2012). This
130 implies that the physical processes underlying any ice thickness changes cannot be examined.
131 Also, the need to run an ensemble of models limits the resolution possible in each case;
132 Massonnet et al. (2013) run 25 ensemble members at 2° resolution.

133

134 The goal of this paper is to produce a high-resolution, free-running, observationally validated
135 hindcast of trends in Antarctic sea ice thickness and volume. This study is complementary to
136 those of Massonnet et al. (2013) and Zhang (in press); the results will not be quantitatively
137 perfect but the use of a free-running (non-data-assimilating) model ensures that thickness
138 trends are the result of calibrated model physics, which we examine in temporal and spatial
139 detail. We place particular emphasis on a detailed assessment of our model results against
140 satellite observations of the mean fields of Antarctic ice concentration, drift, and thickness,
141 and the trend fields of ice concentration and drift. This validation provides a clear view of
142 the relative confidence in the hindcasted ice thickness trends in different regions and seasons.

143

144 **2. Methods**

145 We use revision c62r of the MITgcm (<http://mitgcm.org>) in a regional model of all ocean, sea
146 ice, and ice shelves south of 30°S. The ocean component solves the Boussinesq Navier–
147 Stokes equations on a generalised curvilinear grid using an Arakawa C-grid finite-volume
148 discretisation and z-levels in the vertical (Marshall et al. 1997). All components use the same
149 mesh, with a locally isotropic horizontal resolution of 0.25° in longitude, producing
150 approximately square cells ranging from ~10 km on each side at 70°S to ~18 km at 50°S.
151 The ocean component has 50 vertical levels ranging from 10-m resolution over the top 100 m
152 to 457 m in the layer beneath 5461 m, though the step-like representation of seabed and ice-
153 shelf topography is alleviated by the use of partial cells (Adcroft et al. 1997). Horizontal
154 diffusivity is parameterised following Gent and McWilliams (1990) with a variable
155 diffusivity (Visbeck et al. 1996) (limited to maximum 300 m² s⁻¹) and slope-clipping (Large
156 et al. 1997). Horizontal viscosity is flow-dependent (Leith 1996). Vertical mixing is
157 parameterised according to the ‘K-profile parameterisation’ (KPP) scheme (Large et al.
158 1994), which combines representations of ocean internal mixing and the surface mixed layer,
159 exerting a significant influence upon the sea ice. A fully non-linear equation of state is used
160 (McDougall et al. 2003).

161

162 The sea-ice component (Losch et al. 2010) is also formulated on a C grid. In this study we
163 use an Elastic-Viscous-Plastic procedure to solve for ice dynamics with an elliptic yield
164 curve. Free-slip conditions are applied at boundaries, and ice stress is applied directly to the
165 surface of the ocean. Ice thermodynamics are treated using the ‘zero layer’ approach,
166 employing a constant thermal conductivity and linear temperature profile within the ice
167 (Semtner 1976). The model has only two prognostic ice classes (ice and water) but a linear
168 distribution of 7 thickness classes is used in the thermodynamic calculations. A prognostic
169 snow layer floods into ice if depressed below sea level. Ice salinity is neglected entirely,

170 which implies a slight over-prediction of freshwater fluxes because sea ice is in reality
171 slightly saline. All prognostic variables are transported using first-order upwind advection.
172 Far more sophisticated physical treatments of ice processes are available (Hunke and
173 Lipscomb 2010), and it would be instructive to examine the effect of those in a future study,
174 but the sea ice model is demonstrably able to reproduce the relevant ice observations (see
175 below), so we are confident that its features are sufficient to support the conclusions of this
176 study.

177

178 Initial conditions for ocean temperature and salinity are taken from the World Ocean Atlas
179 (Boyer et al. 2009) (extrapolating southwards where required) and seabed and ice-shelf
180 topography is taken from the RTOPO dataset (Timmermann et al. 2010). Steady
181 climatological boundary conditions are applied at 30°S, with temperature and salinity taken
182 from the World Ocean Atlas and ocean velocities taken from the ECCO2 reanalysis
183 (Menemenlis et al. 2005). The ocean and sea-ice surfaces are forced using 6-hourly fields
184 from the ERA-Interim reanalysis (Dee et al. 2011) at a resolution of 1.5° in both longitude
185 and latitude. The forcing variables consist of zonal and meridional 10-m winds, 2-m air
186 temperature and specific humidity, downward shortwave and longwave radiation, air pressure
187 loading and precipitation. The pressure loading and thermodynamic interactions of static ice
188 shelves are also included (Losch 2008). Iceberg melting is a significant source of freshwater
189 to the Southern Ocean that occurs in a heterogeneous pattern depending upon the distribution
190 of the bergs. We experimented with deriving this flux from third-party model fields, but
191 these were completely dependent upon the modelled bergs and could never be truly
192 representative of the time period used. Therefore, iceberg melting was represented simply by
193 distributing a freshwater flux of 2000 Gt/y uniformly around the coast (Jacobs et al. 1992).
194 No ocean salinity restoring is used.

195

196 The paucity of in-situ atmospheric data over the Southern Ocean means that reanalysis
197 forcing data contain significant biases prior to the onset of satellite sounding data assimilation
198 in late 1978 (Bromwich and Fogt 2004). Therefore, the model is first spun-up by repeating
199 1980 forcings 10 times, and then run forward from 1981 until the end of 2011. Starting the
200 simulations in January avoids the need for any initial sea-ice distribution. Validation of the
201 model against observed ice trends is essential to impart confidence in the modelled ice
202 thickness trends, so we analyse only the period 1992—2010, for which reliable data of trends
203 in ice concentration and drift are available (Holland and Kwok 2012). This provides a total
204 of 22 years of model spin-up time, and we are confident that the trends presented are the
205 result of the atmospheric forcing, not ocean adjustment from initial conditions. In particular,
206 a test simulation in which the 1980 forcings were repeated for 40 years shows no significant
207 sea-ice trends after year 20.

208

209 The model validation requires observations of ice variables on an Antarctic-wide scale. Such
210 observations do not exist directly, but can be derived from quantities observable by satellite.
211 Daily ice concentration data generated from passive microwave emissions using the
212 Bootstrap algorithm are used, with all values below 0.15 masked (Comiso 2000). Ice drift
213 data generated by feature-tracking in the same passive microwave data are also available
214 daily for the entire period, though only from April—October due to a high rejection rate of
215 data in the Austral summer (Holland and Kwok 2012; Kwok et al. 1998). The only
216 comprehensive ice thickness data available on the Antarctic-wide scale are from ICESat laser
217 altimetry campaigns, covering 1—3 one-month-long periods per year for 2003—2008 (Kurtz
218 and Markus 2012). These ice- and snow-thickness data are derived from measurements of
219 freeboard and the assumption that the snow—ice interface is at sea level; i.e. that all

220 freeboard is snow and all draft is solid ice. This assumption is highly questionable in detail,
221 but appears to provide a reasonable level of agreement with in-situ observations overall
222 (Kurtz and Markus 2012; Ozsoy-Cicek et al. 2013; Worby et al. 2008).

223

224 Various definitions of ‘ice thickness’ are used in the literature. Throughout this study,
225 ‘effective ice thickness’ is defined as the volume of ice per unit area of ocean, which is the
226 quantity conserved by the model, while ‘average ice thickness’ is used to refer to the volume
227 of ice per unit area of ice, which is closer to the quantity measured in the field. Effective ice
228 thickness is the product of the average ice thickness and the ice area concentration. We
229 generally investigate fields of effective ice thickness because that is the quantity most
230 relevant to the overall changes in ice volume, but the Antarctic-wide average ice thickness is
231 also examined. We consider the thickness of ice only, rather than including the ice-borne
232 snow layer, because the ice component is of greater interest to many scientific questions, and
233 is also better constrained in our model, which uses uncertain reanalysis precipitation fields to
234 generate ice-borne snow. We consider seasonal maps of means and trends calculated from
235 monthly-mean model output. Mean fields for each season are the overall average of all
236 appropriate months from all years. To produce trend fields, for each grid point we first
237 convert the model output into a timeseries of season-mean values, and then calculate the
238 interannual trend for each season from the appropriate seasonal values over the different
239 years. For example, to calculate the trend in winter ice concentration, we create fields of the
240 mean ice concentration for each winter and then plot, at each grid point, the interannual
241 trends in those fields.

242

243 **3. Results**

244 Before examining our results it is worth considering the extent to which we would expect real
245 ice thickness trends to be represented in a free-running hindcast model. In any model forced
246 by atmospheric reanalyses, ice extent (the ocean area covered by an ice concentration of at
247 least 0.15) should be well-captured; reanalysis models use observed ice concentration in their
248 surface boundary condition, so the ice is imprinted onto their near-surface fields and then
249 recreated in the forced ocean model. However, hindcasting ice area (the area integral of ice
250 concentration) and thickness, hence volume, is more challenging. Antarctic ice drift is
251 dominated by surface winds, and ERA-Interim is known to capture the appropriate wind
252 trends (Holland and Kwok 2012). ERA-Interim air temperatures (Bracegirdle and Marshall
253 2012) and our model ocean temperatures (see below) are also reasonable, implying little
254 limitation on the ice hindcast. However, ice concentration and (crucially) thickness are
255 strongly affected by snow cover (Powell et al. 2005) and ocean freshwater fluxes (Hellmer
256 2004; Zhang 2007), both of which are limited by the large uncertainty in reanalysis
257 precipitation fields (although ERA-Interim is among the best, according to Bromwich et al.
258 (2011)). Also, any convergence-driven dynamical ice thickening will be determined by the
259 assumed rheology of the ice, of which model treatments are uncertain (Feltham 2008;
260 Tsamados et al. 2013). We therefore expect modelled ice thickness trends to be affected by
261 poorly-constrained details of the forcing and models. As a result, we perform a qualitative
262 assessment of our model results against existing observations, and consider broad patterns of
263 ice thickness change rather than quantitative predictions for specific regions, which are
264 perhaps better-provided by the data-assimilating model of Massonnet et al. (2013).

265

266 **3.1 Modelled Ocean Mean State**

267 Since the ocean state and trends can potentially have a significant effect on sea ice, we first
268 assess the mean state of our modelled ocean over the period of interest, 1992-2010 (Figure 1).

269 The long-term mean barotropic streamfunction of the model (Figure 1a) reproduces the
270 observed path of the Antarctic Circumpolar Current (Orsi et al. 1995; Sokolov and Rintoul
271 2009) and, crucially, also captures the shape and strength of the subpolar Weddell and Ross
272 gyres (Wang and Meredith 2008). Thus, to the extent permitted by the sparse available data,
273 we can have some confidence that the dynamic coupling between ocean and ice is accurate.

274

275 The thermodynamic interaction is harder to verify, since there are very few relevant
276 observations of the ocean beneath Antarctic sea ice. Most of our knowledge of ice-ocean
277 interaction comes from summertime observations of the remnant Winter Water and shelf
278 waters formed by winter sea-ice production. As summarised by Petty et al. (submitted), these
279 observations show that in the Weddell and Ross seas the surface mixed layer extends to the
280 seabed in winter, filling the shelf seas with cold and saline shelf waters, while in the
281 Amundsen and Bellingshausen seas the winter mixing only produces a shallower layer of
282 Winter Water, beneath which warmer Circumpolar Deep Water is allowed to persist on the
283 shelf. The mean winter mixed-layer depth (Figure 1b) predicted by the KPP scheme (defined
284 as the shallowest depth for which the overlying bulk Richardson number equals 0.3) shows
285 that the model is able to reproduce these features, with complete destratification in the
286 Weddell and Ross seas and progressively shallower convection in the Amundsen and
287 Bellingshausen seas. This is also reflected in the long-term mean temperature and salinity at
288 the seabed, which shows warm and relatively fresh Circumpolar Deep Water in the
289 Amundsen and Bellingshausen seas and cold and saline shelf waters in the Weddell and Ross
290 seas (Figures 1c and 1d). Further offshore, the winter mixed layer shallows over the sea-ice
291 zone due to a reduction in surface stress and buoyancy forcing, and then deepens offshore of
292 the ice edge. Thus, the vertical structure of the water column seems to compare well to the

293 limited observations that exist, and we infer that the thermodynamic ice-ocean interaction is
294 reasonable as far as it can be tested.

295

296 **3.2 Modelled Ice Mean State**

297 We next compare the mean state of our modelled Antarctic sea ice to observations over the
298 period of interest, 1992-2010. A comparison of mean ice concentration by season (Figure 2)
299 shows that the modelled ice concentration in Austral autumn and winter are very good, which
300 is critical because these seasons have the largest observed ice concentration trends (Turner et
301 al. 2009) and are best covered by ice motion data. Concentrations in spring and summer are
302 not as good, with two persistent problems. Firstly, the model fails to capture a ‘halo’ of low
303 ice concentration near 0°E in spring (Lindsay et al. 2004), which leads to excessive summer
304 ice concentration in the eastern Weddell Sea. The halo is thought to be caused by upward
305 deformation of warm isopycnals near the Maud Rise seamount (de Steur et al. 2007), which
306 is a challenging feature to capture accurately in a large-scale z-level ocean model. Attempts
307 were made to produce this feature using a variety ocean mixing schemes, but these resulted in
308 open-ocean convection and a large polynya in the region (Timmermann and Beckmann
309 2004), strongly degrading the agreement with observations. Secondly, low ice concentrations
310 in the Ross Sea polynya are poorly represented in both spring and summer. Northward ice
311 export in this region is reasonable (see below), so this problem is due to excessive
312 importation of ice from the east.

313

314 A similar comparison of effective ice thickness (Figure 3) shows reasonable results, although
315 some ice concentration errors are also apparent in effective thickness. The model captures
316 the general magnitude of ice thickness and correctly produces thicker ice in the Weddell,
317 Bellingshausen, and Amundsen seas, though the spatial patterns within each region are

318 imperfect. The model under-represents the thickest ice in the north-west corner of the
319 Weddell Sea, though this problem is minimal in autumn, the season of greatest interest here.
320 Ice is too thick in the eastern Weddell Sea, in accordance with the aforementioned lack of
321 halo in this region, and the model over-predicts effective ice thickness in the Ross Sea
322 polynya in all seasons. A similar validation of effective snow thickness (Figure 4) is perhaps
323 worse, with the model failing to reproduce the correct thicknesses in summer and autumn,
324 and producing the wrong pattern in the Weddell Sea in spring. This is unsurprising given the
325 uncertainty surrounding reanalysis precipitation fields, but does place a limitation on our
326 results because snow flooding is an important component of Antarctic sea ice growth (Powell
327 et al. 2005). The model produces a relatively good representation of effective snow thickness
328 in the Pacific sector in spring.

329

330 Given the model's better performance in autumn and winter, and the larger ice trends and
331 greater availability of data in those seasons, the rest of this study concentrates primarily on
332 those seasons. Figure 5 shows the mean ice velocities predicted by the model, which agree
333 with the observations rather well. The focussed northward ice export from the Ross Sea and
334 widespread export in the Weddell Sea are reproduced well, as is the westward coastal current
335 around East Antarctica. Ice drift is a little too rapid near coastlines and the ice edge. This
336 may be a feature of the coarse sampling of the ice observations in these regions, but is more
337 likely to be inaccuracy in the modelled ice dynamics (Uotila et al. submitted). Near the coast
338 this could be caused by problems with the coarse wind forcing or ice rheology. The over-
339 zealous coastal current in the Pacific sector transports too much ice from the Bellingshausen
340 and Amundsen seas into the Ross Sea, explaining the excessive ice concentration in the latter.

341

342 The modelled seasonal cycle in total Antarctic ice area (the area integral of ice concentration)
343 compares extremely well with observations (Figure 6a), which is an important result because
344 ice area is much harder to reproduce in a model than ice extent. The mean cycle of total
345 Antarctic ice volume (Figure 6b) is also in excellent agreement with the data that exist. The
346 modelled Antarctic-wide average ice thickness (total ice volume divided by total ice area;
347 Figure 6b) is remarkably constant throughout the year, varying by less than 20%. This
348 implies that autumn/winter ice thickening is offset by the growth of large areas of thin ice,
349 and spring/summer ice thinning is offset by the melting of large areas of thin ice. The
350 observations suggest the possibility that thicker ice in summer is missed by the model, but
351 this is uncertain because the observations are derived with different assumed values for snow
352 density in each season. If a uniform snow density were used for all seasons, the derived ice
353 thickness would be larger in spring and smaller in summer, in closer agreement with the
354 model.

355

356 **3.3 Modelled Ice Trends**

357 Figure 6 also provides an overview of modelled and observed trends in Antarctic sea ice.
358 Monthly anomalies of ice area from the mean seasonal cycle for the respective datasets are
359 remarkably consistent between model and observations (Figure 6c), with a few exceptions,
360 leading to a good prediction of the overall magnitude of the area trend. Given the difficulty
361 inherent in hindcasting ice area, this is an encouraging result that leads to some confidence in
362 the modelled trends. Building on this confidence, Figure 6d shows a primary conclusion of
363 this model study, that overall Antarctic ice volume and Antarctic-wide average ice thickness
364 have both increased over 1992-2010. The overall volume increase of $29 \text{ km}^3/\text{y}$ is in good
365 agreement with the central Massonnet et al. (2013) estimate of $36 \text{ km}^3/\text{y}$ for 1980—2008
366 using data assimilation. The ice volume anomaly timeseries largely follows that of ice area

367 (Figure 6c), but there are several occasions where anomalies in average ice thickness
368 contribute significantly to ice volume, such as in the prolonged negative anomaly in both
369 variables between 2002 and 2004. As fractions of their mean annual values, the increases in
370 Antarctic average ice thickness ($1.5 \text{ mm/y} / 0.7 \text{ m} \sim 0.2 \text{ \%}/\text{y}$) and total area ($20 \times 10^3 \text{ km}^2/\text{y} /$
371 $10^7 \text{ km}^2 \sim 0.2 \text{ \%}/\text{y}$) contribute equally to the trend in ice volume ($30 \text{ km}^3/\text{y} / 7 \times 10^3 \text{ km}^3 \sim 0.4$
372 \%/y). The Antarctic average ice thickness trend produces a feasible increase of 2.6 cm over
373 the period considered. It is noteworthy that the simulation of Zhang (in press) produces a
374 similar fractional trend in ice volume ($0.46 \text{ \%}/\text{y}$) despite having ice that is approximately
375 double the observed thickness; this suggests that the Zhang (in press) thickness and volume
376 trends are approximately twice the real value (since the extent trend is accurate in that study).
377

378 These overall timeseries hide a strong pattern of regional variation in the trends, much of
379 which compensate, so that the overall Antarctic-mean trends are the residual of much larger
380 regional changes. Figure 7 compares, by season, the maps of linear trend in modelled and
381 observed ice concentration. The general agreement is exceptionally good, with the model
382 clearly reproducing the wave-like pattern of ice concentration trends during this period:
383 decreasing ice cover in Bellingshausen, Weddell, and Mawson seas, and increasing ice cover
384 in Ross, Amundsen, and Cosmonaut seas (Holland and Kwok 2012). The model trends are
385 least reliable in summer, which is unsurprising given the above validation of mean ice
386 concentration in this season. It is interesting to note that the modelled concentration trends
387 seem to be shifted eastwards relative to the observed trends. We cannot be sure why this is,
388 but speculate that the reanalysis winds place the climatological lows in the circumpolar
389 pressure trough (and thus their trends) too far east as a result of poorly representing the
390 deepening of low pressure systems as they navigate Antarctic topography.

391

392 We again restrict our attention to autumn and winter, and investigate the agreement of trends
393 in ice drift between model and observations (Figure 8). Since ice thickness is strongly
394 affected by convergence and divergence, it is essential to have confidence in our modelled
395 ice-drift trends if we are to believe our modelled thickness trends. As shown in Figure 8, the
396 dynamical trends in autumn are in good agreement with observations, particularly
397 considering how challenging it is to correctly model ice velocities, let alone their linear trend.
398 This agreement is largely the result of accurate surface wind trends in ERA-Interim (Holland
399 and Kwok 2012). In autumn the model correctly produces the observed decadal increase in
400 northward ice export in the Ross, Amundsen, and Cosmonaut seas, and the observed decrease
401 in northward export in the Weddell and Mawson seas (Holland and Kwok 2012). Wind and
402 ice-dynamical trends in winter do not fit the observations quite as well, but the broad features
403 of a southward trend in the Bellingshausen Sea and northward trend around 0°E are found in
404 both model and observations.

405

406 These observational assessments of modelled trends in ice concentration and velocity allow
407 us to critically consider the pattern of trends in effective ice thickness (Figure 9) that cause
408 the overall increase in Antarctic sea ice volume. It is immediately apparent that the regional
409 trends in effective ice thickness are at least an order of magnitude larger than the Antarctic-
410 mean trend (Figure 6), which is their residual. The largest effective thickness trends (up to 5
411 cm/y) are found in the Amundsen Sea in winter. This further demonstrates that, while overall
412 Antarctic ice trends may be subtle, the local changes can be of a considerable magnitude.
413 Unsurprisingly, we find that around the ice edge the spatial distribution of effective ice
414 thickness trends (Figure 9) mimics the trends in ice concentration (Figure 8), although there
415 are differences in the relative magnitude of these trends. More importantly, the model also
416 produces effective ice thickness trends in the internal ice pack near the coast, which are not

417 apparent in the concentration trends because the ice is close to full cover throughout the
418 periods considered. These ‘internal’ thickness trends have the largest regional magnitudes,
419 and are an important finding of this study. There are three main regions of internal ice
420 thickness increase: the northwest Weddell Sea in autumn, southern Weddell sea in autumn
421 and winter, and the Amundsen and Bellingshausen seas in winter. Similar trends appear in
422 the model results of Massonnet et al. (2013) and Zhang (in press), though their seasonal
423 structure and physical origin have not been fully examined.

424

425 It is important to note that the maps of trend in effective ice thickness (volume ice per area
426 ocean) are nearly identical to maps of trend in average ice thickness (volume ice per area ice).
427 Away from the ice edge the concentration remains near full cover throughout, so the effective
428 and average thickness are practically the same. Near the ice edge the average ice thickness is
429 of order 10 cm, so the observed changes in ice concentration alone, of order 1%/y, would
430 give a change in effective ice thickness of order 1 mm/y. This is negligible compared to the
431 modelled effective ice thickness changes of order 1 cm/y, which are therefore demonstrated
432 to be the result of large changes in average ice thickness. In other words, the trends in
433 effective ice thickness (volume ice per area ocean) near the ice edge in Figure 9 are
434 negligibly affected by the trends in ice concentration (area ice per area ocean) in Figure 8;
435 they are instead almost entirely trends in average ice thickness (volume ice per area ice). To
436 investigate these trends further we now consider a diagnostic decomposition of the ice-
437 thickness equation.

438

439 **3.4 Analysis of ice trends**

440 An overview of the processes governing the evolution of effective ice thickness can be
441 obtained by separating the total tendency of effective thickness into dynamic and
442 thermodynamic parts. Effective thickness is governed by a simple conservation equation

$$\frac{\partial h}{\partial t} = -\nabla \cdot (\mathbf{u}h) + f$$

443 where h is effective thickness and \mathbf{u} is velocity. The first term on the right-hand side is the
444 thickness change caused by ice-flux divergence, as determined by the momentum balance,
445 while f is the change in thickness due to thermodynamic processes. We record the values of
446 each of these terms separately, and the total tendency, in the ice code. Examination of the
447 mean fields of these tendency terms is highly instructive, as shown in an observational
448 assessment by Holland and Kwok (2012), but here our purpose is to assess trends in ice
449 thickness, for which we assess trends in the tendency terms. This analysis is performed for
450 autumn and winter only, the seasons for which we have greatest confidence in the model
451 results.

452

453 As with all such calculations, maps of interannual trend in the tendency terms are generated
454 by constructing seasonal means of the terms at each grid point and then calculating the
455 interannual trend in the values for each season. The tendency terms represent the rate of
456 change of effective ice thickness during a particular season, so our calculated trends represent
457 the change in that rate over the decadal time period considered. For this reason, the trends in
458 effective ice thickness (e.g. Figure 10a) do not exactly match trends in effective ice thickness
459 tendency (e.g. Figure 10b). The former is the trend in mean autumn effective ice thickness,
460 while the latter is the trend in the mean change in effective ice thickness over autumn. For
461 example, some of the trends in autumn ice thickness are caused by thicker ice being present
462 at the end of summer, and this would cause the two quantities to disagree. However, trends
463 in the autumn effective thickness tendency (Figure 10b) do explain many of the features in

464 the autumn effective thickness trend map (Figure 10a). The only significant regions of
465 disagreement are the areas of ice thickness increase in the southern Amundsen and Ross seas
466 and northwest Weddell Sea, which are therefore revealed to be the result of summertime
467 trends. The model performance is imperfect in summer, so these features should be treated
468 with caution.

469

470 The majority of the trends in effective ice thickness (Figure 10a) are reflected in the trends in
471 effective thickness tendency (Figure 10b), which we can decompose exactly into dynamic
472 (Figure 10c) and thermodynamic (Figure 10d) parts. This decomposition reveals that the
473 trends in the Pacific sector are mostly explained by changes in ice dynamics (compare
474 Figures 10b and 10c). The autumn thickness trend in the southern Weddell Sea is also caused
475 by dynamics, but the thinning in the northern Weddell Sea, and most of the changes around
476 East Antarctica, are due to thermodynamic changes. Changes in wind stress (Figure 10a)
477 succinctly explain all of these changes. In the Amundsen and Ross seas, increased northward
478 ice transport in autumn causes thinning in the south and thickening in the north. In the
479 Bellingshausen Sea, a southward trend in wind stress causes the exact opposite, a loss of ice
480 from the ice edge and a strong thickening near the coast. In the Weddell Sea a decrease in
481 northward ice export away from the coast causes strong thickening. The thermodynamic ice
482 loss to the north could be a result of the decreased export of cold and dry air from Antarctica,
483 or perhaps a southward shift of the warmer waters of the ACC, either of which could be
484 caused by the wind trends. The remaining trends all follow the same pattern of increased
485 (decreased) northward wind stress causing ice thickness increase (decrease) near the ice edge,
486 through a varying combination of changes in air-ice drag and cold- or warm-air advection.
487 These results are in complete agreement with the analysis of Holland and Kwok (2012), who
488 used observations to perform an autumn decomposition of the conservation equation for ice

489 concentration. Wind-driven ice convergence and a resultant thickening in the Pacific sector
490 and southern Weddell Sea were also obtained by Zhang (in press). Finally, we note that the
491 decomposition suggests an increased ice divergence and thermodynamic ice growth in the
492 Ross Sea coastal polynya (Figures 10c and 10d), and a decrease in divergence and growth in
493 the Ronne polynya, Weddell Sea, both in agreement with observed trends (Drucker et al.
494 2011).

495

496 The results in winter (Figure 11) illustrate the difference between trends in effective ice
497 thickness and effective ice thickness tendency. In this season few of the large ice thickness
498 trends (Figure 11a) are observed in the tendency terms (Figure 11b), implying that the
499 thickness trends are the result of changes occurring in previous seasons. For example, the ice
500 thinning trend in the northern Weddell Sea (Figure 11a) is revealed as being a lasting effect
501 of previous seasons; the trend in winter tendency (figure 11b) is towards thickening. On
502 average, there is thinner ice in the northern Weddell Sea during winter, but this ice is
503 thickening more during winter. The ice is thickening less during autumn, and the ice remains
504 thinner during winter as a result. The increased thickening during winter is revealed as being
505 dynamical in origin (figure 11c), because the wind trend in this region is towards increased
506 northward flow (figure 11a).

507

508 Some effective thickness trends that are very clearly caused by wintertime changes are in the
509 Bellingshausen and Amundsen seas, where strong wind trends towards the south lead to a
510 significant winter thickening of the ice near the coast that is entirely dynamic in origin
511 (Figure 11). It is virtually certain that these thickening trends have occurred in reality, since
512 they are the logical extension of known trends in ice concentration, winds, and ice drift in this
513 region (Holland and Kwok 2012; Turner et al. 2009). The model is clearly responding

514 sensibly to the wind stress it receives from ERA-Interim (Figure 11a). However the
515 magnitude and pattern of this thickening must be regarded as merely indicative, for two
516 reasons. Firstly, the ice model cannot be expected to convert wind stress changes into ice
517 thickness changes with a high level of quantitative skill, because this process is heavily
518 dependent upon the poorly constrained rheological properties of the ice (Feltham 2008;
519 Tsamados et al. 2013). Secondly, the detailed pattern of the southward trend in modelled ice
520 motion in this region in winter is imperfect (Figure 8); the observed ice drift trend is towards
521 the Antarctic Peninsula, while the reanalysis wind stress trend (Figure 11a) drives the ice
522 towards the coast in the eastern Bellingshausen Sea and the Amundsen Sea. However, ice
523 drift trends in autumn are well-represented (Figure 8), and these do drive ice westwards in the
524 observations. In summary, the observations strongly support a significant coastal ice
525 thickening in this region, but the model may place it too far east, and with an uncertain
526 magnitude. Massonnet et al. (2013) also model a narrow zone of coastal thickening in this
527 region; Zhang (in press) does not.

528

529 **4. Discussion**

530 The model results presented here reproduce observations of mean ice concentration, drift, and
531 thickness, and trends in ice concentration and drift. The simulated ice thickness trends also
532 agree with those of Massonnet et al. (2013), which can be regarded as a ‘best estimate’ due to
533 their use of data assimilation. This gives us confidence that the physical processes in the
534 model reflect those operating in reality, offering insight into the processes causing trends in
535 Antarctic sea ice. Holland and Kwok (2012) showed that autumn ice concentration trends are
536 dominated by dynamics in the Pacific sector of the Southern Ocean and thermodynamics
537 elsewhere; this modelling study shows that the same pattern holds for ice thickness, and
538 hence ice volume, in autumn and winter.

539

540 This finding has significant consequences. Ice dynamical changes can occur either because
541 the driving stresses have changed, or because the ice is responding differently to a constant
542 stress. The latter can occur if the ice thins, since weaker ice responds more readily to an
543 applied stress, and this is the case in the Arctic, where the ice is accelerating in excess of
544 trends in wind forcing (Kwok et al. 2013). In the Antarctic the trends in ice motion and wind
545 agree closely (Holland and Kwok 2012) and the thickness changes modelled here are much
546 smaller. Thus, the ice-dynamical changes can only ultimately be caused by changes air-ice
547 drag and/or ocean-ice drag, which both ultimately result from changes in the winds since
548 surface ocean currents are predominantly wind-driven. The dynamic origin of the modelled
549 changes in the Pacific sector in autumn and winter therefore implies little or no contribution
550 from changes due to precipitation (Liu and Curry 2010), feedbacks (Stammerjohn et al. 2012;
551 Zhang 2007), or atmosphere or ocean warming (Jacobs and Comiso 1997; Lefebvre and
552 Goosse 2005; Liu et al. 2004). This certainly does not rule out a contribution from these
553 mechanisms in summer and spring, or around East Antarctica. A detailed analysis of the
554 trends in ice thermodynamics, in a model capable of accurately representing the warmer
555 seasons, is clearly required to advance this question.

556

557 The results also suggest that it is unlikely that increased ice-sheet melting is implicated in the
558 Antarctic sea ice increase, as proposed by Bintanja et al. (2013). The vast majority of
559 increased freshwater discharge from the Antarctic Ice Sheet has entered the Amundsen Sea
560 (Shepherd et al. 2012) and followed the coastal current westward into the Ross Sea, where it
561 has caused a significant freshening (Jacobs and Giulivi 2010). If ice-shelf meltwater were to
562 contribute to the sea-ice trends, the largest effect would thus be expected to occur in the
563 increasing ice volume in the western Pacific. Our results, and the observational analysis of

564 Holland and Kwok (2012), show quite clearly that the trends in that region are predominantly
565 dynamic in origin in autumn and winter. In addition, the model presented here has no overall
566 trend in ice-sheet meltwater input (the prescribed iceberg discharge is steady, and total ice-
567 shelf melting contains no significant trend), yet is able to reproduce most features of the
568 observed Antarctic ice concentration increase. Thus our results are in agreement with the
569 study of Swart and Fyfe (2013), who found that the Antarctic sea ice trends were not affected
570 by trends in Antarctic Ice Sheet freshwater flux.

571

572 **5. Conclusions**

573 There are no observations of decadal trends in Antarctic sea ice thickness and volume, so we
574 hindcast them for the period 1992—2010 using a numerical ice—ocean model that is
575 extensively validated against observations. The model accurately simulates mean fields of
576 ice concentration, drift, and thickness in autumn and winter, and reproduces observed trends
577 in ice concentration and drift. This validation allows us to hold some confidence in the
578 corresponding modelled trends in ice thickness.

579

580 Unsurprisingly, the model shows that the observed ice-concentration trends near the ice edge
581 have corresponding trends in ice thickness, with areas of increasing thickness associated with
582 increasing concentration. Model diagnostics show that these thickness trends are driven
583 dynamically in the Pacific sector and thermodynamically elsewhere, in agreement with an
584 observational decomposition of ice concentration trends (Holland and Kwok 2012). The
585 model also reveals that the observed southward trends in ice drift in the Bellingshausen and
586 Weddell seas have caused ice to thicken near the coast, a trend that does not appear in ice
587 concentration measurements because the ice remains at full cover throughout. The Weddell
588 Sea thickening occurs in response to decreased export early in the year, while the

589 Bellingshausen Sea thickening occurs in winter due to a strong trend towards southward ice
590 flow. These results are the logical extension of known trends in ice concentration, winds, and
591 ice drift. The dynamic origin of the autumn and winter trends in the Pacific sector imply that
592 they must be forced by changes in the winds, rather than other atmospheric or oceanic
593 forcings or feedbacks.

594

595 Spatial patterns of increasing and decreasing trends in ice concentration and thickness largely
596 compensate, so that neither variable has a large Antarctic trend overall. Thickening in the
597 interior of the ice pack enhances the overall thickness trend relative to the concentration
598 trend. As fractions of their mean annual values, the modelled increases in Antarctic-wide ice
599 thickness ($1.5 \text{ mm/y} \sim 0.2 \text{ \%/y}$) and area ($20 \times 10^3 \text{ km}^2/\text{y} \sim 0.2 \text{ \%/y}$) contribute equally to the
600 overall trend in ice volume ($30 \text{ km}^3/\text{y} \sim 0.4 \text{ \%/y}$). This small gain contrasts markedly with
601 the observed Arctic sea ice volume loss of $500\text{--}1000 \text{ km}^3/\text{y}$ ($\sim 3\text{--}6 \text{ \%/y}$) (Kwok and
602 Rothrock 2009; Laxon et al. 2013). In terms of Southern Ocean freshwater forcing, the small
603 increase in sea ice freshwater extraction is outweighed by the $\sim 70 \text{ km}^3/\text{y}$ increase in
604 freshwater input from the Antarctic Ice Sheet (Shepherd et al. 2012).

605

606 **References**

607 Adcroft, A., C. Hill, and J. Marshall, 1997: Representation of topography by shaved cells in a
608 height coordinate ocean model. *Mon Weather Rev*, **125**, 2293-2315.

609 Bintanja, R., G. J. van Oldenburgh, S. S. Drijfhout, B. Wouters, and C. A. Katsman, 2013:
610 Important role for ocean warming and increased ice-shelf melt in Antarctic sea-ice expansion.
611 *Nature Geosci.*

612 Bitz, C. M., P. R. Gent, R. A. Woodgate, M. M. Holland, and R. Lindsay, 2006: The
613 influence of sea ice on ocean heat uptake in response to increasing CO₂. *J Climate*, **19**, 2437-
614 2450.

615 Boyer, T., and Coauthors, 2009: World Ocean Database 2009, NOAA Atlas NESDIS 66, 216
616 pp.

617 Bracegirdle, T. J., and G. J. Marshall, 2012: The Reliability of Antarctic Tropospheric
618 Pressure and Temperature in the Latest Global Reanalyses. *J Climate*, **25**, 7138-7146.

619 Bromwich, D. H., and R. L. Fogt, 2004: Strong trends in the skill of the ERA-40 and NCEP-
620 NCAR reanalyses in the high and midlatitudes of the southern hemisphere, 1958-2001. *J*
621 *Climate*, **17**, 4603-4619.

622 Bromwich, D. H., J. P. Nicolas, and A. J. Monaghan, 2011: An Assessment of Precipitation
623 Changes over Antarctica and the Southern Ocean since 1989 in Contemporary Global
624 Reanalyses. *J Climate*, **24**, 4189-4209.

625 Cavalieri, D. J., and C. L. Parkinson, 2012: Arctic sea ice variability and trends, 1979-2010.
626 *Cryosphere*, **6**, 881-889.

627 Comiso, J. C., 2000: Bootstrap Sea Ice Concentrations from Nimbus-7 SMMR and DMSP
628 SSM/I-SSMIS. Version 2. [1992-2010 used]. National Snow and Ice Data Center, Boulder,
629 Colorado, USA.

630 Comiso, J. C., and F. Nishio, 2008: Trends in the sea ice cover using enhanced and
631 compatible AMSR-E, SSM/I, and SMMR data. *J Geophys Res*, **113**, C02s07.

632 de Steur, L., D. M. Holland, R. D. Muench, and M. G. McPhee, 2007: The warm-water
633 "Halo" around Maud Rise: Properties, dynamics and Impact. *Deep-Sea Res I*, **54**, 871-896.

634 Dee, D. P., and Coauthors, 2011: The ERA-Interim reanalysis: configuration and
635 performance of the data assimilation system. *Q J Roy Meteor Soc*, **137**, 553-597.

636 Drucker, R., S. Martin, and R. Kwok, 2011: Sea ice production and export from coastal
637 polynyas in the Weddell and Ross Seas. *Geophys Res Lett*, **38**, Artn L17502.

638 Feltham, D. L., 2008: Sea ice rheology. *Annu Rev Fluid Mech*, **40**, 91-112.

639 Fichefet, T., B. Tartinville, and H. Goosse, 2003a: Antarctic sea ice variability during 1958-
640 1999: A simulation with a global ice-ocean model. *J Geophys Res*, **108**.

641 Fichefet, T., H. Goosse, and M. A. M. Maqueda, 2003b: A hindcast simulation of Arctic and
642 Antarctic sea ice variability, 1955-2001. *Polar Res*, **22**, 91-98.

643 Gent, P. R., and J. C. McWilliams, 1990: Isopycnal Mixing in Ocean Circulation Models. *J*
644 *Phys Oceanogr*, **20**, 150-155.

645 Giles, K. A., S. W. Laxon, and A. P. Worby, 2008: Antarctic sea ice elevation from satellite
646 radar altimetry. *Geophys Res Lett*, **35**, L03503.

647 Hellmer, H. H., 2004: Impact of Antarctic ice shelf basal melting on sea ice and deep ocean
648 properties. *Geophys Res Lett*, **31**, L10307.

649 Holland, P. R., and R. Kwok, 2012: Wind-driven trends in Antarctic sea ice drift. *Nature*
650 *Geosci*, 10.1038/ngeo1627.

651 Hunke, E., and W. H. Lipscomb, 2010: CICE: the Los Alamos Sea Ice Model Documentation
652 and Software User's Manual Version 4.1, LA-CC-06-012.

653 Jacobs, S. S., and J. C. Comiso, 1997: Climate variability in the Amundsen and
654 Bellingshausen Seas. *J Climate*, **10**, 697-709.

655 Jacobs, S. S., and C. F. Giulivi, 2010: Large Multidecadal Salinity Trends near the Pacific-
656 Antarctic Continental Margin. *J Climate*, **23**, 4508-4524.

657 Jacobs, S. S., H. H. Helmer, C. S. M. Doake, A. Jenkins, and R. M. Frolich, 1992: Melting of
658 Ice Shelves and the Mass Balance of Antarctica. *J Glaciol*, **38**, 375-387.

659 Kurtz, N. T., and T. Markus, 2012: Satellite observations of Antarctic sea ice thickness and
660 volume. *J Geophys Res*, **117**, C08025.

661 Kwok, R., and D. A. Rothrock, 2009: Decline in Arctic sea ice thickness from submarine and
662 ICESat records: 1958-2008. *Geophys Res Lett*, **36**, L15501.

663 Kwok, R., G. Spreen, and S. Pang, 2013: Arctic sea ice circulation and drift speed: Decadal
664 trends and ocean currents. *J Geophys Res*, **118**, 2408-2425.

665 Kwok, R., A. Schweiger, D. A. Rothrock, S. Pang, and C. Kottmeier, 1998: Sea ice motion
666 from satellite passive microwave imagery assessed with ERS SAR and buoy motions. *J*
667 *Geophys Res*, **103**, 8191-8214.

668 Large, W. G., J. C. McWilliams, and S. C. Doney, 1994: Oceanic Vertical Mixing - a Review
669 and a Model with a Nonlocal Boundary-Layer Parameterization. *Rev Geophys*, **32**, 363-403.

670 Large, W. G., G. Danabasoglu, S. C. Doney, and J. C. McWilliams, 1997: Sensitivity to
671 surface forcing and boundary layer mixing in a global ocean model: Annual-mean
672 climatology. *J Phys Oceanogr*, **27**, 2418-2447.

673 Laxon, S. W., and Coauthors, 2013: CryoSat-2 estimates of Arctic sea ice thickness and
674 volume. *Geophys Res Lett*, **40**, 732-737.

675 Lefebvre, W., and H. Goosse, 2005: Influence of the Southern Annular Mode on the sea ice-
676 ocean system: the role of the thermal and mechanical forcing. *Ocean Science*, **1**, 145-157.

677 ———, 2008: An analysis of the atmospheric processes driving the large-scale winter sea ice
678 variability in the Southern Ocean. *J Geophys Res*, **113**, Artn C02004.

679 Leith, C. E., 1996: Stochastic models of chaotic systems. *Physica D*, **98**, 481-491.

680 Lindsay, R. W., D. M. Holland, and R. A. Woodgate, 2004: Halo of low ice concentration
681 observed over the Maud Rise seamount. *Geophys Res Lett*, **31**.

682 Liu, J. P., and J. A. Curry, 2010: Accelerated warming of the Southern Ocean and its impacts
683 on the hydrological cycle and sea ice. *P Natl Acad Sci USA*, **107**, 14987-14992.

684 Liu, J. P., J. A. Curry, and D. G. Martinson, 2004: Interpretation of recent Antarctic sea ice
685 variability. *Geophys Res Lett*, **31**, Artn L02205.

686 Losch, M., 2008: Modeling ice shelf cavities in a z coordinate ocean general circulation
687 model. *J Geophys Res*, **113**, C08043.

688 Losch, M., D. Menemenlis, J. M. Campin, P. Heimbach, and C. Hill, 2010: On the
689 formulation of sea-ice models. Part 1: Effects of different solver implementations and
690 parameterizations. *Ocean Model*, **33**, 129-144.

691 Mahlstein, I., P. R. Gent, and S. Solomon, 2013: Historical Antarctic mean sea ice area, sea
692 ice trends, and winds in CMIP5 simulations. *J Geophys Res-Atmos*, **118**.

693 Markus, T., R. Massom, A. Worby, V. Lytle, N. Kurtz, and T. Maksym, 2011: Freeboard,
694 snow depth and sea-ice roughness in East Antarctica from in situ and multiple satellite data.
695 *Ann Glaciol*, **52**, 242-248.

696 Marshall, J., A. Adcroft, C. Hill, L. Perelman, and C. Heisey, 1997: A finite-volume,
697 incompressible Navier Stokes model for studies of the ocean on parallel computers. *J*
698 *Geophys Res*, **102**, 5753-5766.

699 Massonnet, F., P. Mathiot, T. Fichefet, H. Goosse, C. K. Beatty, M. Vancoppenolle, and T.
700 Lavergne, 2013: A model reconstruction of the Antarctic sea ice thickness and volume
701 changes over 1980-2008 using data assimilation. *Ocean Model*, **64**, 67-75.

702 Mathiot, P., C. K. Beatty, T. Fichefet, H. Goosse, F. Massonnet, and M. Vancoppenolle,
703 2012: Better constraints on the sea-ice state using global sea-ice data assimilation. *Geosci*
704 *Model Dev*, **5**, 1501-1515.

705 McDougall, T. J., D. R. Jackett, D. G. Wright, and R. Feistel, 2003: Accurate and
706 computationally efficient algorithms for potential temperature and density of seawater. *J*
707 *Atmos Ocean Tech*, **20**, 730-741.

708 Menemenlis, D., and Coauthors, 2005: NASA supercomputer improves prospects for ocean
709 climate research. *Eos Transactions*, **86**.

710 Orsi, A. H., T. Whitworth, and W. D. Nowlin, 1995: On the Meridional Extent and Fronts of
711 the Antarctic Circumpolar Current. *Deep-Sea Res I*, **42**, 641-673.

712 Ozsoy-Cicek, B., S. F. Ackley, H. Xie, D. Yi, and H. J. Zwally, 2013: Sea ice thickness
713 retrieval algorithms based on in situ surface elevation and thickness values for application to
714 altimetry. *J Geophys Res*, **118**, 3807-3822.

715 Parkinson, C. L., and D. J. Cavalieri, 2012: Antarctic sea ice variability and trends, 1979-
716 2010. *Cryosphere*, **6**, 871-880.

717 Petty, A. A., P. R. Holland, and D. L. Feltham, submitted: Sea ice and the ocean mixed layer
718 over the Antarctic shelf seas. *The Cryosphere*.

719 Polvani, L. M., and K. L. Smith, 2013: Can natural variability explain observed Antarctic sea
720 ice trends? New modeling evidence from CMIP5. *Geophys Res Lett*, **40**, 3195-3199.

721 Powell, D. C., T. Markus, and A. Stossel, 2005: Effects of snow depth forcing on Southern
722 Ocean sea ice simulations. *J Geophys Res*, **110**.

723 Semtner, A., 1976: A model for the thermodynamic growth of sea ice in numerical
724 investigations of climate. *J Phys Oceanogr*, **6**, 379-389.

725 Shepherd, A., and Coauthors, 2012: A Reconciled Estimate of Ice-Sheet Mass Balance.
726 *Science*, **338**, 1183-1189.

727 Sigmond, M., and J. C. Fyfe, 2010: Has the ozone hole contributed to increased Antarctic sea
728 ice extent? *Geophys Res Lett*, **37**.

729 Sokolov, S., and S. R. Rintoul, 2009: Circumpolar structure and distribution of the Antarctic
730 Circumpolar Current fronts: 1. Mean circumpolar paths. *J Geophys Res*, **114**, C11018.

731 Stammerjohn, S. E., R. Massom, D. Rind, and D. G. Martinson, 2012: Regions of rapid sea
732 ice change: an inter-hemispheric seasonal comparison. *Geophys Res Lett*, **39**, Artn L06501.

733 Stammerjohn, S. E., D. G. Martinson, R. C. Smith, X. Yuan, and D. Rind, 2008: Trends in
734 Antarctic annual sea ice retreat and advance and their relation to El Nino-Southern
735 Oscillation and Southern Annular Mode variability. *J Geophys Res*, **113**, Artn C03s90.

736 Stossel, A., Z. R. Zhang, and T. Vihma, 2011: The effect of alternative real-time wind forcing
737 on Southern Ocean sea ice simulations. *J Geophys Res*, **116**.

738 Swart, N. C., and J. C. Fyfe, 2013: The influence of recent Antarctic ice sheet retreat on
739 simulated sea ice area trends. *Geophys Res Lett*, **40**, 4328-4332.

740 Timmermann, R., and A. Beckmann, 2004: Parameterization of vertical mixing in the
741 Weddell Sea. *Ocean Model*, **6**, 83-100.

742 Timmermann, R., A. Beckmann, and H. H. Hellmer, 2002: Simulations of ice-ocean
743 dynamics in the Weddell Sea 1. Model configuration and validation. *J Geophys Res*, **107**.

744 Timmermann, R., A. Worby, H. Goosse, and T. Fichefet, 2004: Utilizing the ASPeCt sea ice
745 thickness data set to evaluate a global coupled sea ice-ocean model. *J Geophys Res*, **109**.

746 Timmermann, R., H. Goosse, G. Madec, T. Fichefet, C. Etche, and V. Duliere, 2005: On the
747 representation of high latitude processes in the ORCA-LIM global coupled sea ice-ocean
748 model. *Ocean Model*, **8**, 175-201.

749 Timmermann, R., S. Danilov, J. Schroter, C. Boning, D. Sidorenko, and K. Rollenhagen,
750 2009: Ocean circulation and sea ice distribution in a finite element global sea ice-ocean
751 model. *Ocean Model*, **27**, 114-129.

752 Timmermann, R., and Coauthors, 2010: A consistent data set of Antarctic ice sheet
753 topography, cavity geometry, and global bathymetry. *Earth Syst. Sci. Data*, **2**, 261-273.

754 Tsamados, M., D. L. Feltham, and A. V. Wilchinsky, 2013: Impact of a new anisotropic
755 rheology on simulations of Arctic sea ice. *Journal of Geophysical Research*, **118**, 91-107.

756 Turner, J., T. Bracegirdle, T. Phillips, G. J. Marshall, and J. S. Hosking, 2012: An initial
757 assessment of Antarctic sea ice extent in the CMIP5 models. *J Climate*, **26**, 1473-1484.

758 Turner, J., and Coauthors, 2009: Non-annular atmospheric circulation change induced by
759 stratospheric ozone depletion and its role in the recent increase of Antarctic sea ice extent.
760 *Geophys Res Lett*, **36**, Artn L08502.

761 Uotila, P., P. R. Holland, T. Vihma, S. J. Marsland, and N. Kimura, submitted: Is realistic
762 Antarctic sea ice extent in climate models the result of excessive ice drift? *Ocean Model*.

763 Visbeck, M., J. Marshall, and H. Jones, 1996: Dynamics of isolated convective regions in the
764 ocean. *J Phys Oceanogr*, **26**, 1721-1734.

765 Wang, Z., and M. P. Meredith, 2008: Density-driven Southern Hemisphere subpolar gyres in
766 coupled climate models. *Geophys Res Lett*, **35**, L14608.

767 Worby, A. P., C. A. Geiger, M. J. Paget, M. L. Van Woert, S. F. Ackley, and T. L. DeLiberty,
768 2008: Thickness distribution of Antarctic sea ice. *J Geophys Res*, **113**.

769 Xie, H., E. Emre Tekeli, S. F. Ackley, D. Yi, and H. J. Zwally, 2013: Sea ice thickness
770 estimations from ICESat altimetry over the Bellingshausen and Amundsen seas, 2003-2009. *J*
771 *Geophys Res*, **118**, 2438-2453.

772 Zhang, J. L., 2007: Increasing Antarctic sea ice under warming atmospheric and oceanic
773 conditions. *J Climate*, **20**, 2515-2529.

774 ———, in press: Modeling the impact of wind intensification on Antarctic sea ice volume. *J*
775 *Climate*.

776 Zunz, V., H. Goosse, and F. Massonnet, 2013: How does internal variability influence the
777 ability of CMIP5 models to reproduce the recent trend in Southern Ocean sea ice extent?
778 *Cryosphere*, **7**, 451-468.

779 Zwally, H. J., D. H. Yi, R. Kwok, and Y. H. Zhao, 2008: ICESat measurements of sea ice
780 freeboard and estimates of sea ice thickness in the Weddell Sea. *J Geophys Res*, **113**.

781 Zwally, H. J., J. C. Comiso, C. L. Parkinson, D. J. Cavalieri, and P. Gloersen, 2002:
782 Variability of Antarctic sea ice 1979-1998. *J Geophys Res*, **107**, Artn 3041.

783

784 **Figure Captions**

785

786 Figure 1: Modelled mean 1992-2010 ocean fields. a) Barotropic stream function (contours
787 every 10 Sv, magenta contour 0 Sv), b) Winter (JJA) mean mixed-layer depth from KPP
788 calculation (contours every 25 m, magenta contour 100 m), c) Potential temperature at seabed
789 (contours every 0.2 °C, magenta contour 0 °C), d) Salinity at seabed (contours every 0.025,
790 magenta contour 34.65).

791

792 **Figure 2:** Modelled and observed 1992-2010 mean ice concentration by season. Observed ice
793 concentration is calculated using the Bootstrap algorithm (Comiso 2000). WS: Weddell Sea,
794 CS: Cosmonaut Sea, MS: Mawson Sea, RS: Ross Sea, AS: Amundsen Sea, BS:
795 Bellingshausen Sea.

796

797 **Figure 3:** Modelled mean 1992-2010 effective ice thickness and observed mean 2003-2008
798 effective ice thickness by season. Effective ice thickness is defined as volume of ice per unit
799 area of ocean, neglecting the ice-borne snow layer. Observed effective ice thickness is
800 derived from ICESat measurements (Kurtz and Markus 2012). Areas with respective ice
801 concentration below 0.5 are masked in both datasets.

802

803 **Figure 4:** Modelled mean 1992-2010 effective snow thickness and observed mean 2003-2008
804 effective snow thickness by season. Effective snow thickness is defined as volume of ice-
805 borne snow per unit area of ocean. Observed effective snow thickness is derived from
806 ICESat measurements (Kurtz and Markus 2012). Areas with respective ice concentration
807 below 0.5 are masked in both datasets.

808

809 Figure 5: Modelled and observed 1992-2010 mean ice concentration and ice drift for autumn
810 and winter seasons. Observed ice concentration is calculated using the Bootstrap algorithm
811 (Comiso 2000) and ice velocities are from passive microwave feature-tracking (Holland and
812 Kwok 2012). Model velocities are shown every tenth grid point.

813

814 Figure 6: 1992-2010 temporal variability of total Antarctic sea ice variables from model and
815 observation. a) mean seasonal cycle in total ice area (the area integral of ice concentration)
816 for model and observations (Comiso 2000). b) mean seasonal cycle in total ice volume and
817 mean ice thickness (total ice volume divided by total ice area) for model and observations
818 (dots represent individual ICESat campaigns, shaded areas represent interannual mean \pm
819 standard deviation for each season; Kurtz and Markus (2012)). c) monthly anomalies in
820 modelled and observed total ice area from respective climatologies in panel a. d) monthly
821 anomalies in modelled total ice volume and mean ice thickness from respective climatologies
822 in panel b. All trends shown are significant at the 99% level.

823

824 Figure 7: Modelled and observed 1992-2010 linear trends in ice concentration by season.
825 Observed ice concentration is calculated using the Bootstrap algorithm (Comiso 2000).

826

827 Figure 8: Modelled and observed 1992-2010 linear trends in ice concentration and drift for
828 autumn and winter seasons. Observed ice concentration is calculated using the Bootstrap
829 algorithm (Comiso 2000) and ice velocities are from passive microwave feature-tracking
830 (Holland and Kwok 2012). Model velocities are shown every tenth grid point.

831

832 Figure 9: Modelled 1992-2010 linear trends in effective ice thickness and drift for autumn
833 and winter seasons. Effective ice thickness is defined as volume of ice per unit area of ocean,
834 neglecting the ice-borne snow layer. Model velocities are shown every tenth grid point. The
835 largest trends, up to 5 cm/y, are in the Amundsen Sea in winter.

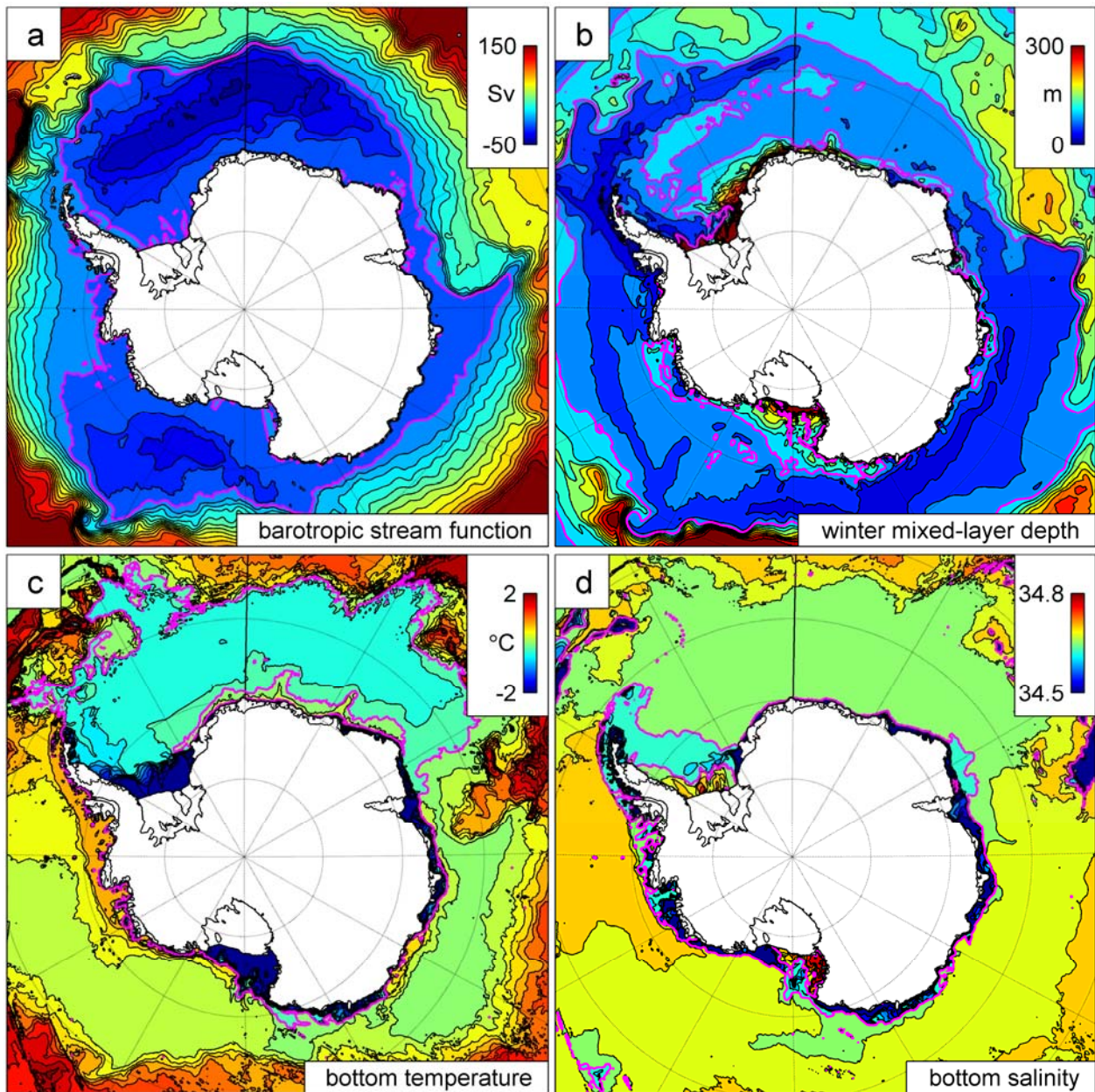
836

837 Figure 10: Modelled autumn (AMJ) 1992-2010 linear trends in effective ice thickness and
838 related quantities. a) trends in modelled effective ice thickness and ERA-Interim wind stress
839 (shown every tenth grid point); b) trends in evolution term in ice-thickness equation; c) trends
840 in dynamic part of ice-thickness evolution; d) trends in thermodynamic part of ice-thickness
841 evolution. The colourbar for panels c and d is the same as for panel b.

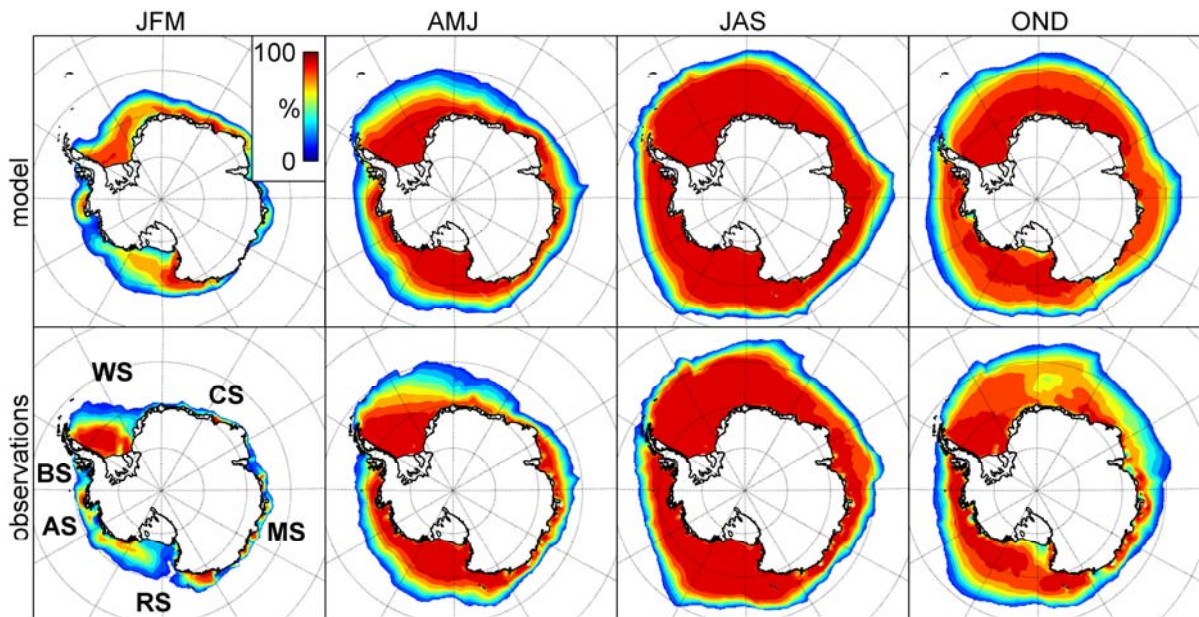
842

843 Figure 11: As Figure 10 but for winter (JAS).

844

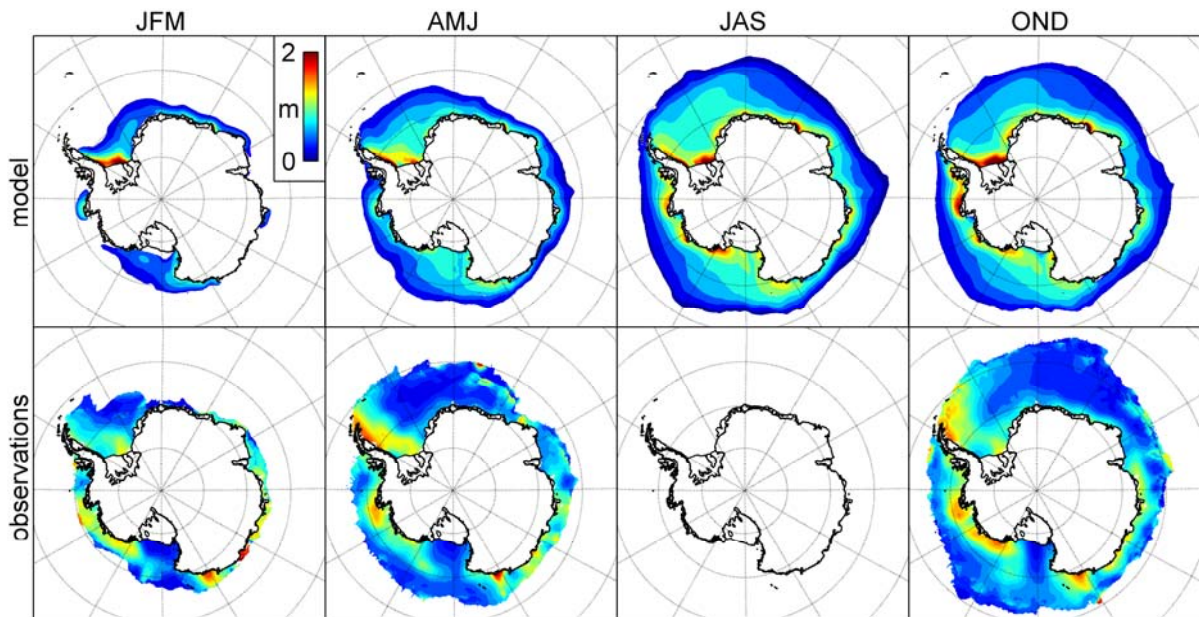


845 Figure 1: Modelled mean 1992-2010 ocean fields. a) Barotropic stream function (contours
 846 every 10 Sv, magenta contour 0 Sv), b) Winter (JJA) mean mixed-layer depth from KPP
 847 calculation (contours every 25 m, magenta contour 100 m), c) Potential temperature at seabed
 848 (contours every 0.2 °C, magenta contour 0 °C), d) Salinity at seabed (contours every 0.025,
 849 magenta contour 34.65).



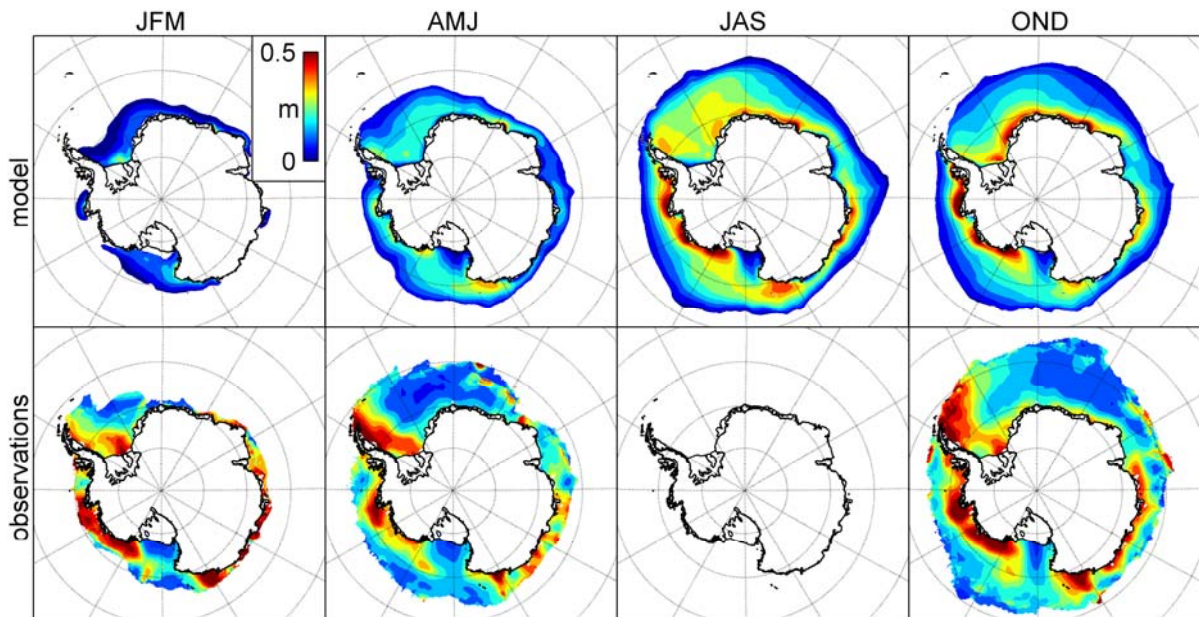
850 Figure 2: Modelled and observed 1992-2010 mean ice concentration by season. Observed ice
 851 concentration is calculated using the Bootstrap algorithm (Comiso 2000). WS: Weddell Sea,
 852 CS: Cosmonaut Sea, MS: Mawson Sea, RS: Ross Sea, AS: Amundsen Sea, BS:
 853 Bellingshausen Sea.

854



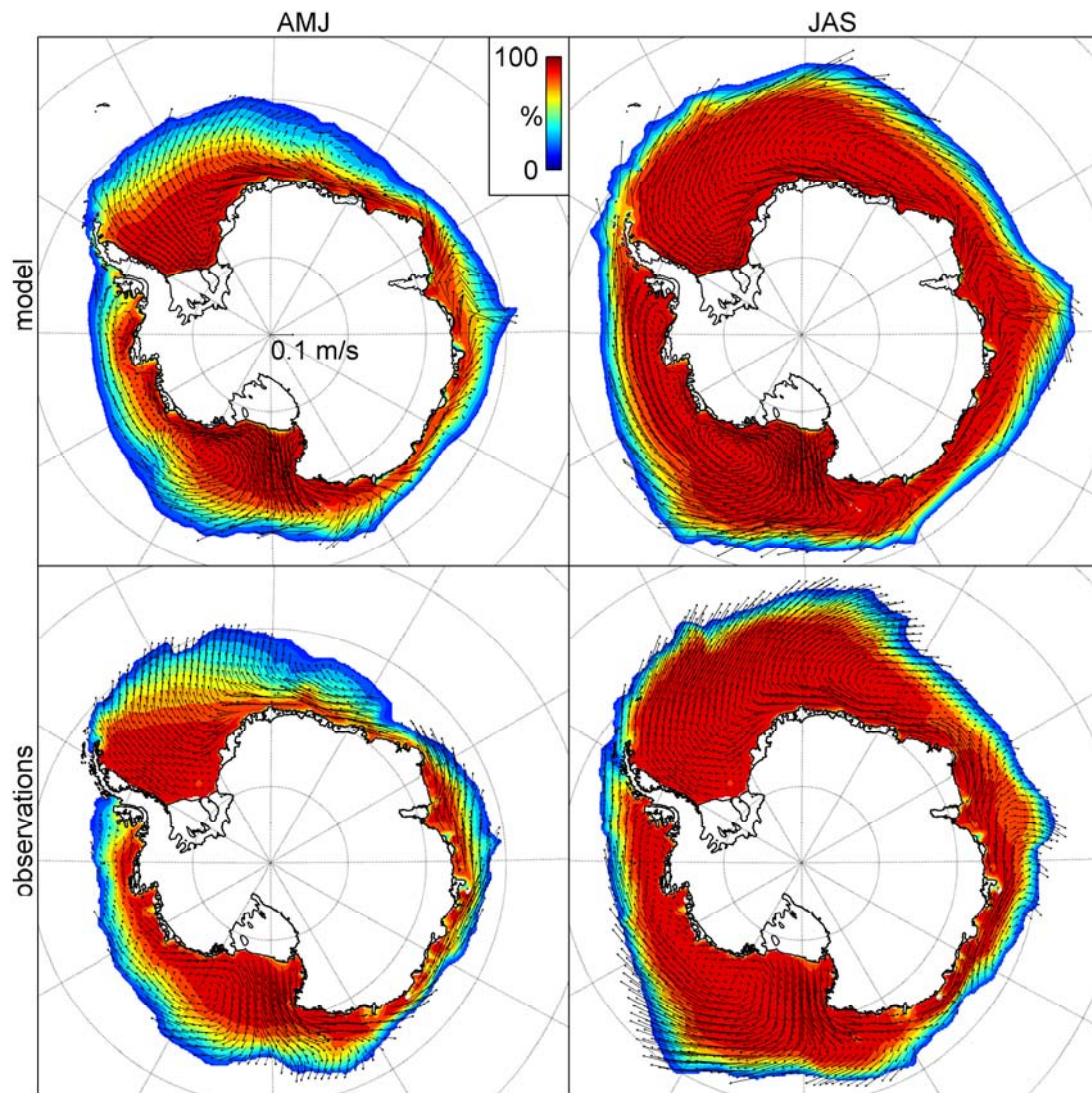
855 Figure 3: Modelled mean 1992-2010 effective ice thickness and observed mean 2003-2008
 856 effective ice thickness by season. Effective ice thickness is defined as volume of ice per unit
 857 area of ocean, neglecting the ice-borne snow layer. Observed effective ice thickness is
 858 derived from ICESat measurements (Kurtz and Markus 2012). Areas with respective ice
 859 concentration below 0.5 are masked in both datasets.

860



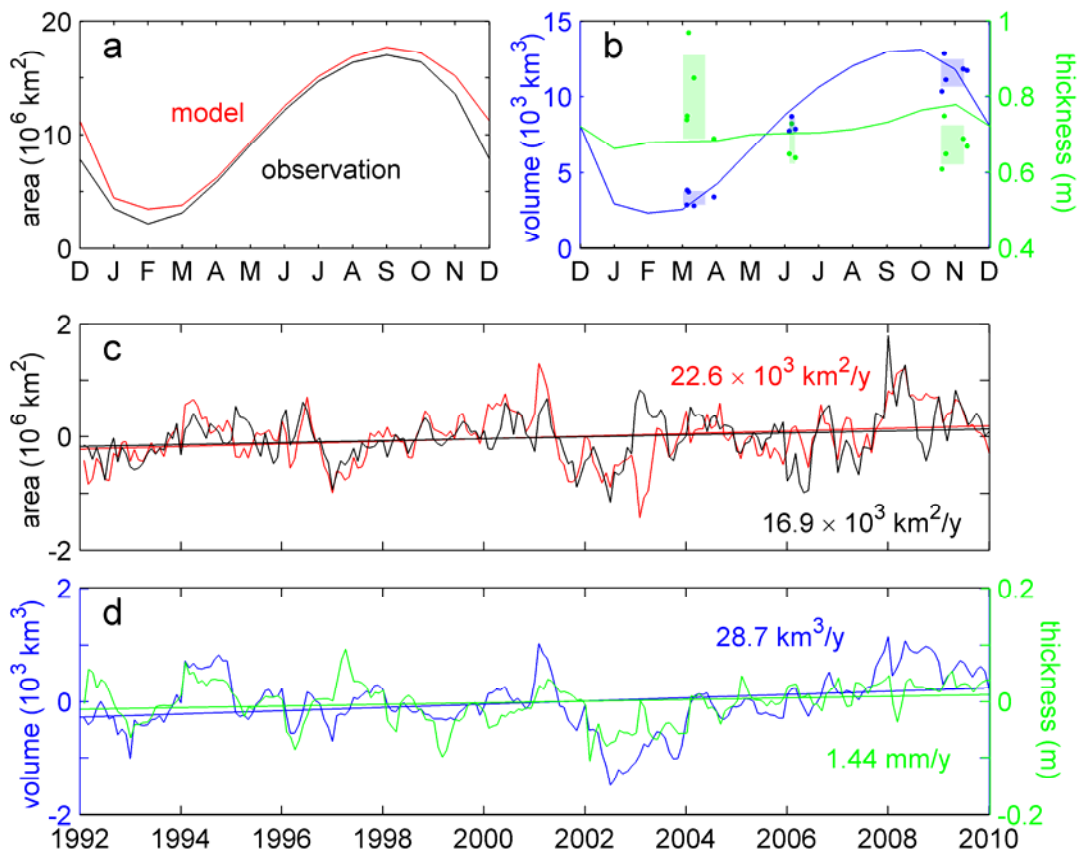
861 Figure 4: Modelled mean 1992-2010 effective snow thickness and observed mean 2003-2008
 862 effective snow thickness by season. Effective snow thickness is defined as volume of ice-
 863 borne snow per unit area of ocean. Observed effective snow thickness is derived from
 864 ICESat measurements (Kurtz and Markus 2012). Areas with respective ice concentration
 865 below 0.5 are masked in both datasets.

866



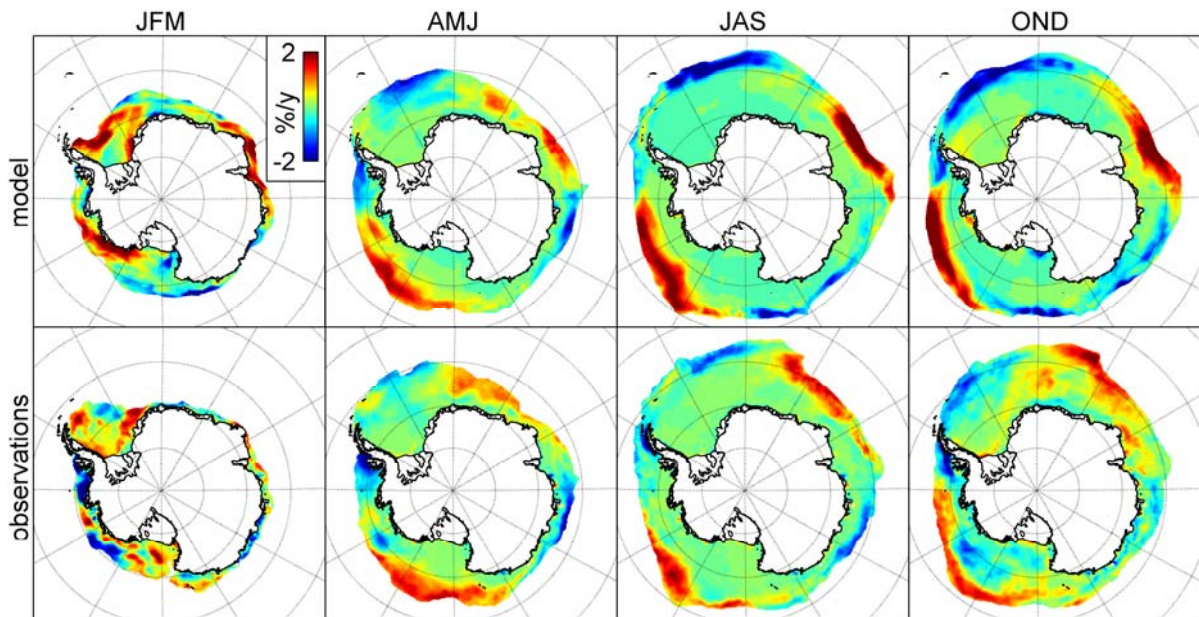
867 Figure 5: Modelled and observed 1992-2010 mean ice concentration and ice drift for autumn
 868 and winter seasons. Observed ice concentration is calculated using the Bootstrap algorithm
 869 (Comiso 2000) and ice velocities are from passive microwave feature-tracking (Holland and
 870 Kwok 2012). Model velocities are shown every tenth grid point.

871



872 Figure 6: 1992-2010 temporal variability of total Antarctic sea ice variables from model and
 873 observation. a) mean seasonal cycle in total ice area (the area integral of ice concentration)
 874 for model and observations (Comiso 2000). b) mean seasonal cycle in total ice volume and
 875 mean ice thickness (total ice volume divided by total ice area) for model and observations
 876 (dots represent individual ICESat campaigns, shaded areas represent interannual mean \pm
 877 standard deviation for each season; Kurtz and Markus (2012)). c) monthly anomalies in
 878 modelled and observed total ice area from respective climatologies in panel a. d) monthly
 879 anomalies in modelled total ice volume and mean ice thickness from respective climatologies
 880 in panel b. All trends shown are significant at the 99% level.

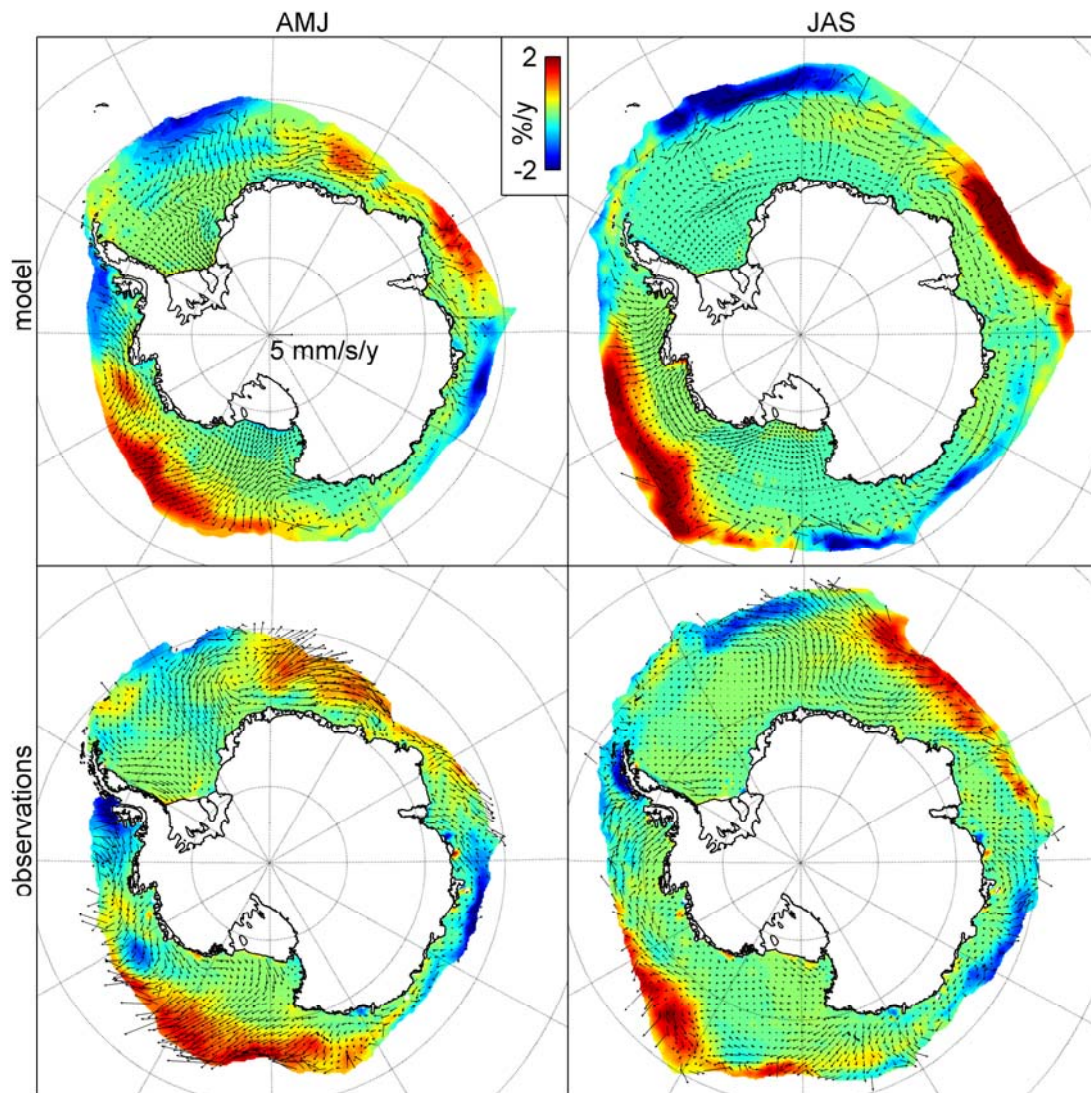
881



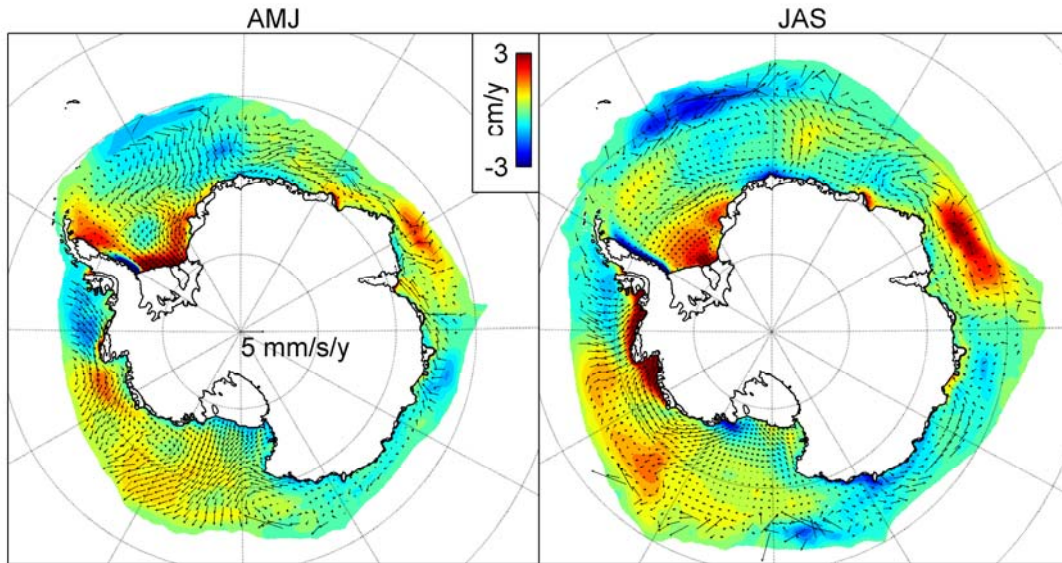
882 Figure 7: Modelled and observed 1992-2010 linear trends in ice concentration by season.

883 Observed ice concentration is calculated using the Bootstrap algorithm (Comiso 2000).

884

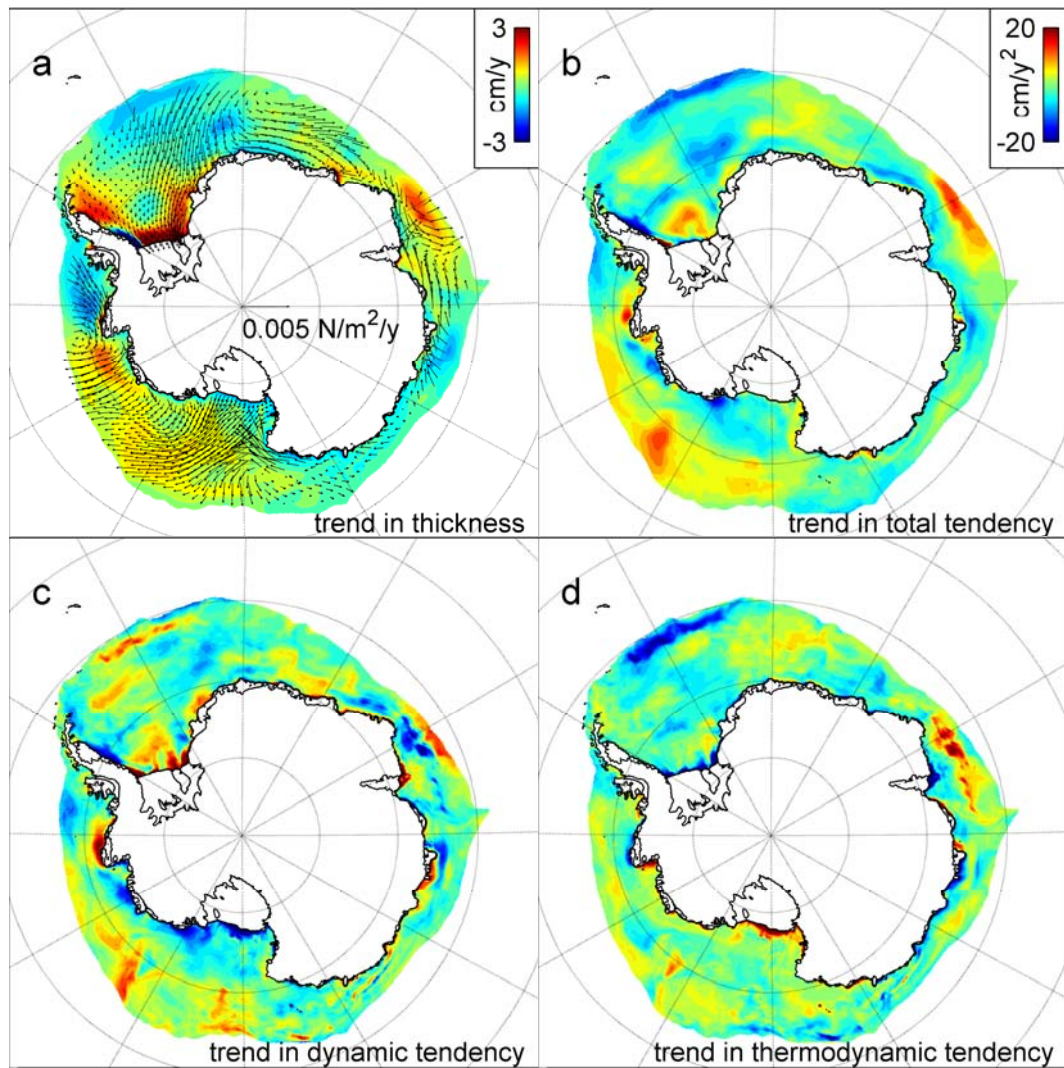


885 Figure 8: Modelled and observed 1992-2010 linear trends in ice concentration and drift for
 886 autumn and winter seasons. Observed ice concentration is calculated using the Bootstrap
 887 algorithm (Comiso 2000) and ice velocities are from passive microwave feature-tracking
 888 (Holland and Kwok 2012). Model velocities are shown every tenth grid point.
 889

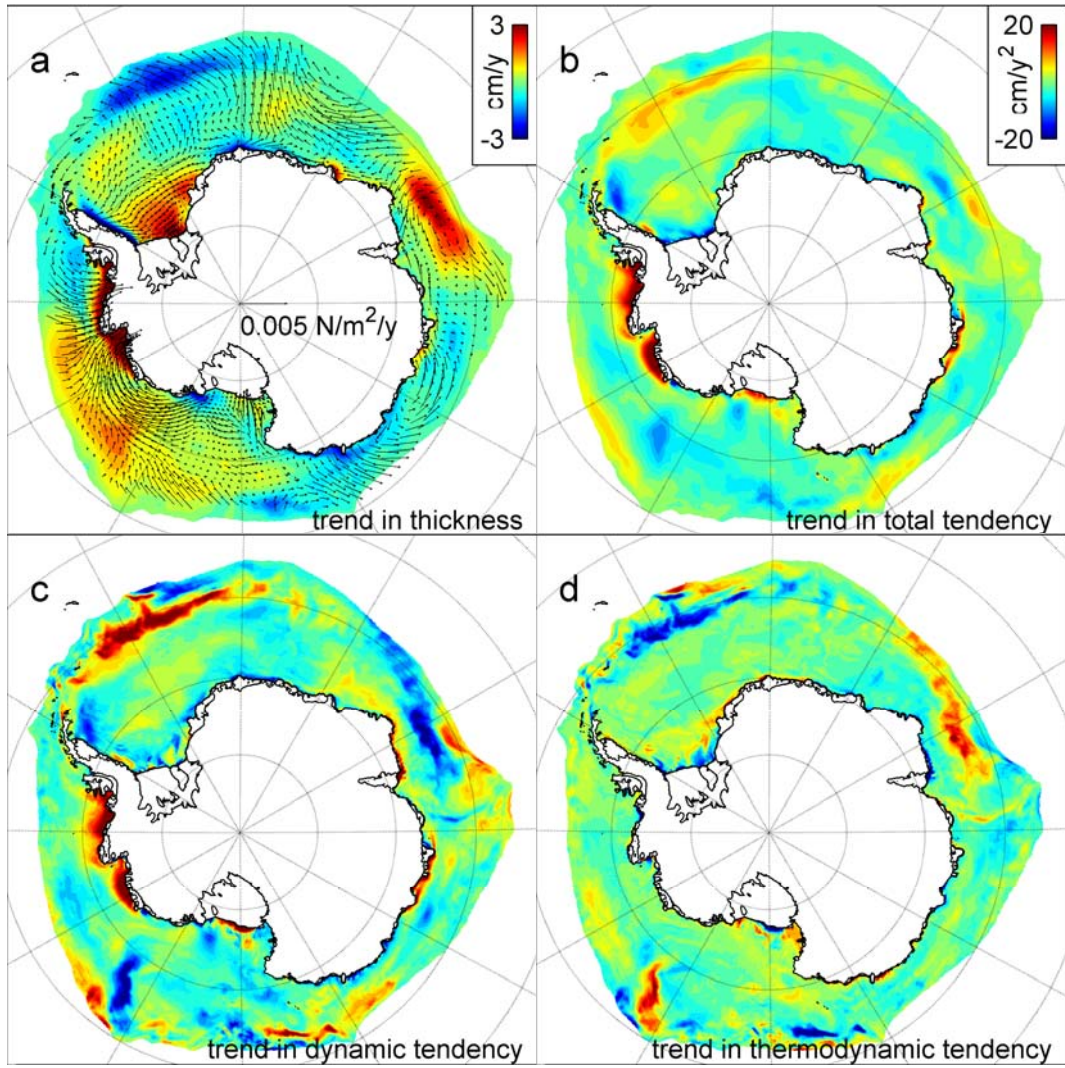


890 Figure 9: Modelled 1992-2010 linear trends in effective ice thickness and drift for autumn
 891 and winter seasons. Effective ice thickness is defined as volume of ice per unit area of ocean,
 892 neglecting the ice-borne snow layer. Model velocities are shown every tenth grid point. The
 893 largest trends, up to 5 cm/y, are in the Amundsen Sea in winter.

894



895 Figure 10: Modelled autumn (AMJ) 1992-2010 linear trends in effective ice thickness and
 896 related quantities. a) trends in modelled effective ice thickness and ERA-Interim wind stress
 897 (shown every tenth grid point); b) trends in evolution term in ice-thickness equation; c) trends
 898 in dynamic part of ice-thickness evolution; d) trends in thermodynamic part of ice-thickness
 899 evolution. The colourbar for panels c and d is the same as for panel b.
 900



901 Figure 11: As Figure 10 but for winter (JAS).